Supplemental Document

Quantitative 3D refractive index tomography of opaque samples in epi-mode: supplement

PATRICK LEDWIG AND FRANCISCO E. ROBLES*

Coulter Department of Biomedical Engineering, Georgia Institute of Technology and Emory University, Atlanta, Georgia 30332, USA
**Corresponding author: robles@gatech.edu*

Supplement DOI: https://doi.org/10.6084/m9.figshare.13259933

Parent Article DOI: https://doi.org/10.1364/OPTICA.410135

Quantitative 3D refractive index tomography of opaque samples in epi-mode: supplemental material

This document provides supplemental information to "3D refractive index tomography in thick scattering samples in epi-mode with quantitative oblique back-illumination microscopy". This document contains figures and information regarding further validation of the reconstruction method in the presence of an inhomogeneous scatterer, the effect of scaling photon transport simulation geometry fidelity, and a demonstration of an iterative linear reconstruction with a total-variation constraint in dense scattering tissue.

1. VALIDATION OF BRAIN TISSUE AS A SCATTERING SOURCE

While the reconstruction of polystyrene beads was performed to validate the qOBM 3D method in the presence of a uniform, well-defined intralipid scattering medium, the same could be shown for an inhomogeneous scattering medium like those natively present *in-vivo* and in bulk biological tissue samples. In order to validate the reconstruction with such an inhomogeneous scattering source, we performed a bead reconstruction experiment analogous to those previously performed with an intralipid scattering phantom, but instead with a freshly-excised rat brain as the surrounding medium. This brain sample was coronally sectioned at the mid-line and placed on a coverslip on top of the 100 μm well containing the nearly index-matched thermoplastic medium (n=1.533 at 720 nm) and the 10 μm polystyrene beads in the same configuration as the intralipid phantom, which provided a semi-diffuse scattering light source for the beads. Furthermore, this experiment was performed in simulation, with a voxelized model rat brain rendered and used as a scattering medium in the Monte Carlo photon transport simulation (MCX, Monte Carlo eXtreme [1]), the results of which were used to produce a system transfer function. Finally the imaging system was simulated with a partially coherent forward model. For further details, see section 4 of the main text.

Reconstruction of the bead's 3D refractive index was performed (see Fig. S1). Listed in order of appearance in Fig. S1 from left to right, the figure shows the original differential phase contrast image (DPC), as a set of 2D stacks (2D), using a direct 3D Tikhonov deconvolution (3D TK) and finally using an iterative total-variation and non-negativity constrained 3D deconvolution (3D TV). The time taken to perform each of the three reconstruction operations in MATLAB (volume dimensions 165x165x141 pixels) were 0.333 seconds, 0.223 seconds, and 83 seconds, for the 2D, 3D TK, and 3D TV, respectively, with the two direct methods (2D and 3D TK) being performed on CPU (12 core, 3.8 GHz, AMD Ryzen X3900) and the iterative method (3D TV) accelerated with a GPU (nVidia GeForce RTX 2080 Ti). The slight improvement in computation time between 3D TK over 2D TK comes from the improved efficiency of a vectorized implementation in MATLAB, in spite of the increased computational complexity of a 3D FFT, which has time complexity $O(N\ log\ N)$, where N is the number of data points, regardless of dimensionaliy[2].

As before, the beads' 1D center traces in the lateral plane were much more accurate than the same in the X-Z longitudinal plane for all reconstructions due to the missing cone effect of transmissive microscopy. Furthermore, the image quality and numerical accuracy of the reconstructions were no worse than those for the previous reconstructions with intralipid phantoms. This supports our use of a transfer function based on brain optical scattering parameters for further experiments, and suggests that the degree of complexity of the background scattering medium is immaterial to the success of the qOBM reconstruction, as long as it is accounted for in the photon transport simulation.

Given these results, it is natural to ask to what extent must the voxelized geometry used in simulation resemble the actual physical properties of the experiment it is replicating, both in shape and scattering parameters, in order to produce a reliable result. If the qOBM reconstruction is robust to inaccuracies in the simulation model, it may be advantageous to model a homogeneous semi-infinite slab with bulk scattering properties taken *en masse* in place of a detailed voxelized geometry, which may require heavier computation and may not be readily available for many realistic *in situ* and *in vivo* samples. This is discussed below in Supplemental Section 2.

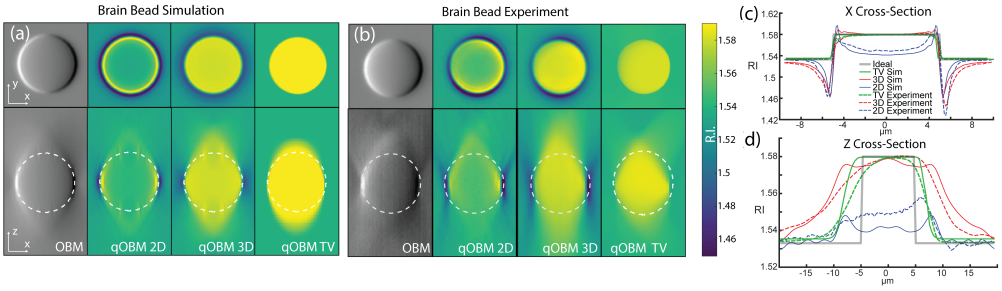

Fig. S1. Bead simulation (a) and experimental results (b) of z-stacks of 10 μm polystyrene bead underneath a section of unaltered rat brain. Cross-sections through the imaging plane (X-Y) are shown on top and through the axial plane (X-Z) are shown on bottom. -Y) are shown on top and through the axial plane (X-Z) are shown on bottom. From left to right, the images show a volume rendition of bead using OBM, 2D effective RI reconstruction, direct Tikhonov 3D RI reconstruction, and iterative total-variation-constrained 3D RI reconstruction. (c) Center trace through x axis demonstrating halo-artifact reduction by the 3D reconstruction. (d) Center trace through z-axis.

2. EFFECT OF SIMULATION FIDELITY ON SOURCE INTENSITY PROFILE

To demonstrate the degree of sensitivity of the qOBM reconstruction to variations in agreement between the simulated model and the real-world experimental set-up, we reconstructed a section of the rat brain tissue with a transfer function produced from a full voxelized model of a rat brain [3] (Fig. S2b), and then compared it to a reconstruction produced from a semi-infinite slab model of gray-matter tissue. These models, therefore, disagreed in both geometrical shape and voxel-wise scattering parameters (again, one model is a homogeneous slab and the other a complex 3D brain model). All other experimental parameters are equal, including the axial tilt angle, distance, and wavelength of the illuminating source LEDs. In addition, the regularization parameter was held constant.

Results are shown in Figs. S2a and c, which show the projected 2D and 1D angular intensity profiles of the multiply scattered light captured in simulation. Gray matter produces an illumination profile that is very similar to the voxelized model (Fig. S2a). A comparison to a semi-infinite slab of white matter is also provided and shows nearly identical results to the voxelized model (Fig S2c), due to the volumetric preponderance of white matter in the brain.

Figures S2d and e demonstrate qOBM's robustness to variations in model-experiment agreement. Here 3D qOBM reconstructions of brain tissue using a transfer function produced from the semi-infinite slab of gray-matter (Fig. S2d) and from the voxelized brain model (Fig. S2e) show nearly identical results. The difference in measured refractive index values between these two cross-sections is minimal ($\lesssim$0.001). It can therefore be reasonably assumed that the quantitative 3D refractive index maps produced by 3D qOBM in experiment do not deviate far enough from those that would be produced by a more detailed simulation volume to justify the replication of a volume more complex than the semi-infinite gray-matter slab that was used.

A final note on potential variations of the angular distribution of light used to estimate the transfer function of the system deals with depth dependence. Indeed the angular distribution will change with depth. However, the depth at which significant angular variations will begin to occur—-that would in-turn significantly affect the transfer function—-will be at depths much larger than the penetration depth of the qOBM system which is currently about $\sim$100 µm. For scale, this distance roughly corresponds to the edge length of a single voxel in a high-fidelity Monte Carlo simulation geometry.

3. DEGREE OF SUCCESS OF ITERATIVE RECONSTRUCTION

Apart from simulation model fidelity, the results of the bead experiments shown in Fig. S1 further raise the question of the necessity of a sparsity-based total variation-constrained iterative reconstruction of a complex biologically-relevant 3D volume such as the one shown in Fig. 3 in the main text. While the center traces show that TV reconstruction produces a compensation in axial diffraction in both the brain-illuminated beads in Figs. S1 c and d and the intralipid-illuminated beads shown Figs. 2c and d of the main text, it comes at a heavy computational cost (372-fold in

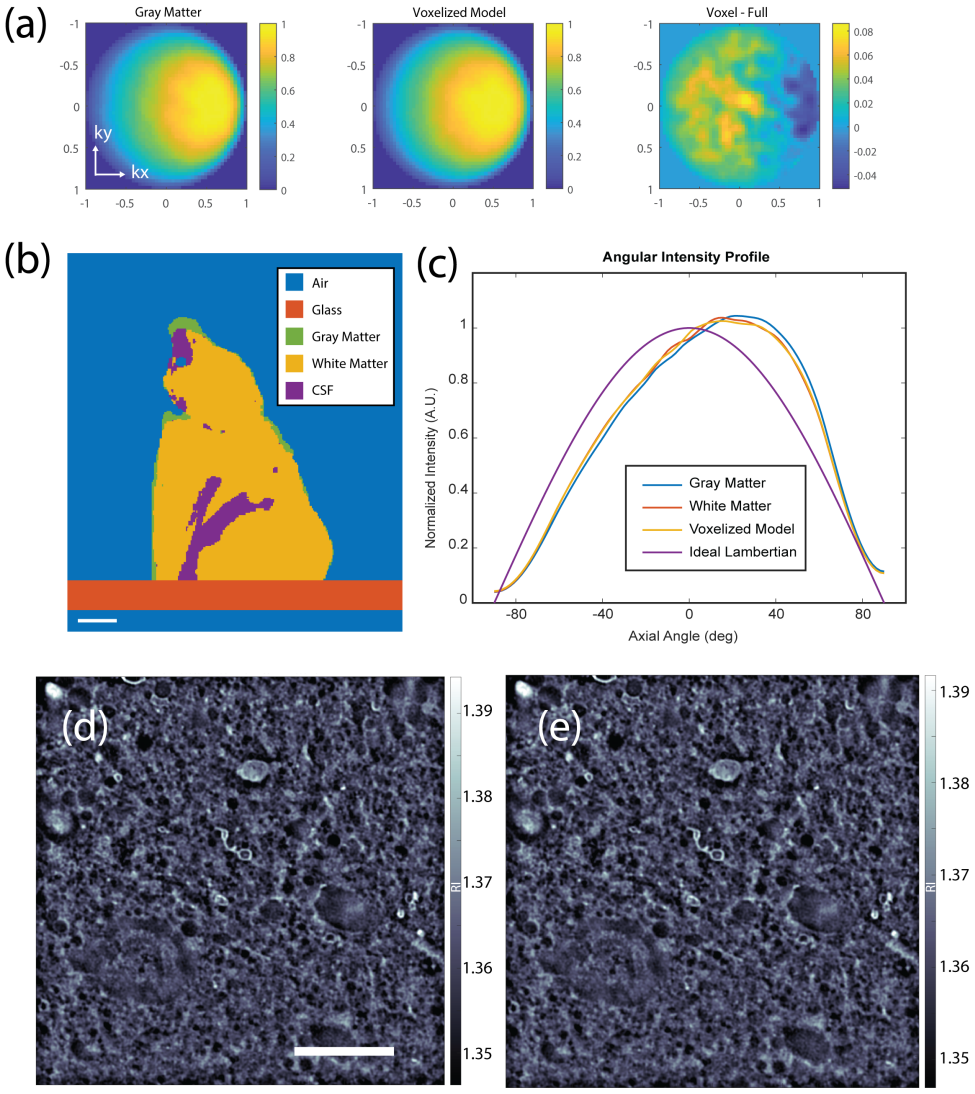

Fig. S2. (a) The angular distribution of light intensity as a result of Monte-Carlo photon transport simulation through a semi-infinite gray-matter slab versus a full voxelized model of a rat brain. (b) Cross-section of simulation geometry demonstrating degree of detail. Scale bar is 2 mm. (c) Intensity profile of effective source in axial angle along the forward azimuthal angle between the source and the detector. (d,e) En-face brain image reconstructed using OTF generated with a gray-matter only model and full voxelized model, respectively. The striking similarity indicates a robustness to imperfect simulation parameters. Scale bar is 20 μm.

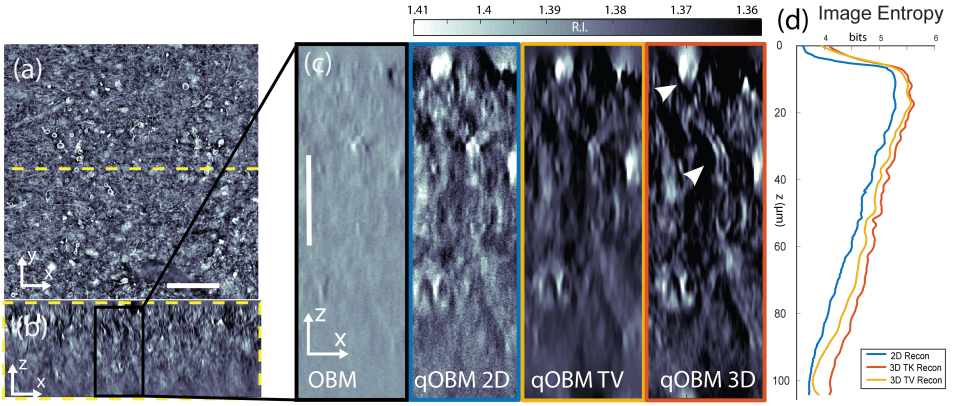

Fig. S3. Human brain biopsy (cortex) repeated from Fig. 3 in the main text. (a) Representative *en face* slice at 48μm depth. Scale bar is 50 μm. (b) Side central cross-section at yellow dashed line in (a), at same scale as (a). (d) Enlarged selected region from (c). From left to right, the images represent the same region from a conventional OBM reconstruction, 2D qOBM, qOBM TV and qOBM 3D reconstructions, respectively. Arrows indicate a pooled red blood cell (top), and an axially traversing axon cross-section. Scale bar is 25 μm.(d) Graph of entropy, an indicator of information quantity in an image, of cross-sectional *en-face* images as a function of depth for the reconstruction methods shown.

our implementation). Furthermore the benefits are most apparent only in the nearly-homogeneous bead sample, which inherently has a low amount of total spatial variation. For a thick volumetric sample (243x243x104 μm^3 in Fig. S3), an iterative method is computationally prohibitive, as the data quantity prohibits the acceleration with the GPU. Furthermore, a densely featured biological sample such as a section of brain is much less sparse in its actual refractive index map than a single polystyrene bead or a minimally scattering sample that is typically prepared from conventional tomographic phase microscopy, such as a single cell or microorganism. For that reason, conventional approaches for tomographic phase reconstruction may need to be re-evaluated before being applied to qOBM.

It stands to reason, then, that the total variation-constrained reconstruction that is a keystone of conventional tomographic phase microscopy [4] would be less effective for partially-coherent illumination in the scattering volumes under investigation in this work. Indeed, after a portion of the sample (80x80x104 μm^3) in Fig, S3a is reconstructed and compared in axial profile to the standard direct Tikhonov reconstruction, it fails to highlight important details, such as the ascending axon in Fig. S3c, to the same degree as the direct reconstruction. When this comparison is extended to the axial plane, as in Fig S4a and b, it can be seen that the total variation reconstruction (second column) smooths over subtle details from the dense underbrush of dendritic cellular projections that the direct regularized 3D (third column) and even 2D (first column) deconvolution methods preserve. Furthermore, the smoothing is amplified deeper into the tissue (Fig. S4c), where the SNR is diminished due to the accumulation of second scattering events between the plane of observation and the camera (Fig. S4e). This is demonstrated by the linear drop in entropy, a measure of image information[5] with depth, consistent with a volume with constant scattering parameters.

The computation times of the region of interest shown in Fig. S4 (704x704x299 voxels) were 15 seconds, 10 seconds, and 108 minutes for the 2D, 3D TK, and iterative 3D TV reconstructions, respectively. Again, the improvement in computation time in the 3D TK reconstruction over 2D TK reconstruction comes from the improved efficiency of a vectorized implementation in MATLAB. In the case of 3D TV here, memory restrictions prevented GPU acceleration of the iterative reconstruction, so the computational cost increase further compounded to a 648-fold increase. Clearly, for the given computational investment, a reconstruction approach that is more directly suitable to partially-coherent phase imaging is needed in order to enhance the results of direct Tikhonov deconvolution.

Finally, other computational methods can be implemented. Given that there is a direct parallel between qOBM and the treatment of transmission-based 3D RI systems, more complex

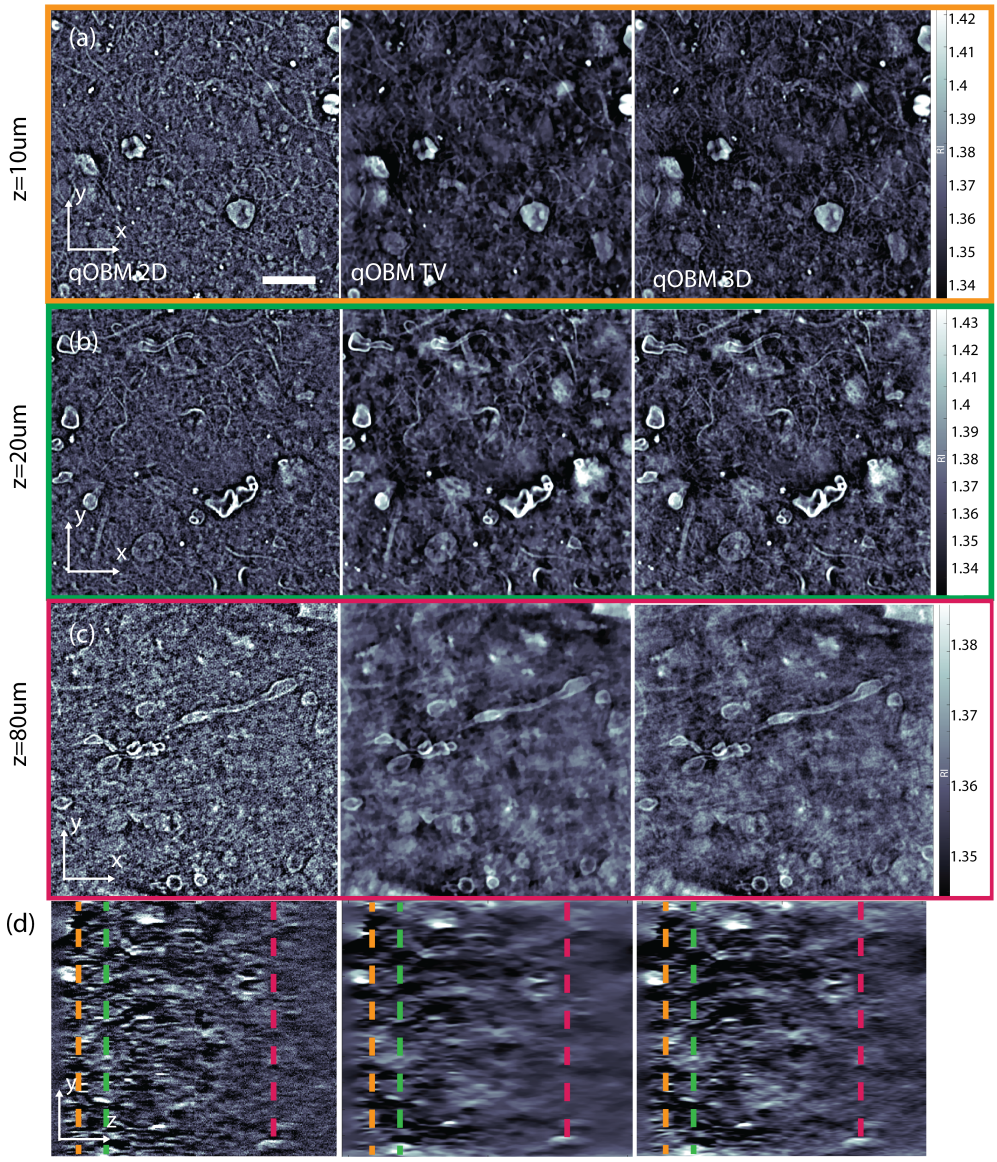

Fig. S4. Portion of Human brain biopsy (cortex) repeated from Fig. 3 in the main text. (a) En-face view (x-y) of tissue at a 10 micron-depth, reconstructed with (from left to right) 2D qOBM, qOBM 3D TV, and qOBM 3D TK, respectively. (b,c) The same as (a), but at 20 μm and 80 μm depths, respectively. (d) Vertical cross-section (y-z) from same region, containing highlighted region in fig. S3. Dashed lines indicate depth shown in images shown with corresponding colored border.

models that, for example, take multiple-scattering into account [6, 7] may be within reach some modifications. This is part of our future work.

4. A NOTE ON THE VALIDITY OF THE FIRST BORN APPROXIMATION

In the polystyrene bead reconstruction experiments shown in Fig. S1 and Fig. 2 of the main text, a surrounding medium was chosen with an index of refraction of 1.533, while the index of refraction of a 10 μm polystyrene bead is 1.581 at 720 nm [8]. The conventional heuristic for determining the validity of the 1st Born approximation for holographic techniques has been given by weak object criterion:[9]

$$k\,\Delta n\,a \ll 1, \tag{S1}$$

where a is the radius of the refracting object, and k is the wavenumber. This term is found by evaluating the convergence of the Born series at the center of the refracting object where the field is most likely to diverge, providing a strong theoretical constraint on the approximation. With this criterion, our bead sample would result in an evaluation of 2.1, apparently exceeding the region of convergence of the Born series.

However, in 2009, Trattner *et al.* showed that for wide-field phase-contrast microscopy, the convergence of the Born series needs only to be evaluated at the point of detection of the field, specifically the objective lens, where the criteria for weak scattering was found to be given by the less restrictive criterion [10]

$$\left|\frac{k^2}{4\pi r}(n_1^2 - n_0^2)V\right| \ll 1, \tag{S2}$$

where r is the working distance of the microscope (2mm for our instrument), and V is the volume of the refracting element (the polystyrene bead in this case). With the weak-scattering criterion given by Eqn. S2, convergence of the Born series is implied, and for the bead experiments considered in this work, this evaluates to 0.23. This easily clears the criterion, validating the use of the 1st Born model and weak-object assumption. It likewise explains the consistent results between the partially-coherent forward model simulation and the experimental images, along with the concomitant lack of refractive artifacts despite a seemingly large index of refraction disparity and bead radius. Moreover, for the biological samples shown in this work, the constraints on scattering are less restrictive than the polystyrene beads since biological structures in tissues have a much smaller optical volume (product of physical volume and change in index of refraction).

While a Rytov approximation-based approach has been suggested to provide more consistent results in biological samples when applied to coherent tomographic reconstruction methods [4], it was shown in Ref. [11] that in the partially-coherent case, this approach produces the same weak-object transfer function as the Born approach, but with additional constraints on object scattering. Therefore a Born-theoretic analysis was deemed adequate for this work, given the convenient avenue for analysis it provides.

REFERENCES

1. Q. Fang and D. A. Boas, "Monte Carlo Simulation of Photon Migration in 3D Turbid Media Accelerated by Graphics Processing Units," Opt. Express **17**, 20178 (2009).
2. R. N. R. N. Bracewell, *The Fourier transform and its applications* (McGraw Hill, 2000).
3. Y. Liu, S. L. Jacques, M. Azimipour, J. D. Rogers, R. Pashaie, and K. W. Eliceiri, "OptogenSIM: a 3D Monte Carlo simulation platform for light delivery design in optogenetics," Biomed. Opt. Express **6**, 4859 (2015).
4. D. Jin, R. Zhou, Z. Yaqoob, and P. T. C. So, "Tomographic phase microscopy: principles and applications in bioimaging [Invited]," J. Opt. Soc. Am. B **34**, B64 (2017).
5. C. E. Shannon, "A Mathematical Theory of Communication," Bell Syst. Tech. J. (1948).
6. J. Lim, A. B. Ayoub, E. E. Antoine, and D. Psaltis, "High-fidelity optical diffraction tomography of multiple scattering samples," Light. Sci. & Appl. **8**, 1–12 (2019).
7. S. Chowdhury, M. Chen, R. Eckert, D. Ren, F. Wu, N. Repina, and L. Waller, "High-resolution 3D refractive index microscopy of multiple-scattering samples from intensity images," Optica **6**, 1211 (2019).
8. N. Sultanova, S. Kasarova, and I. Nikolov, "Dispersion properties of optical polymers," in *Acta Physica Polonica A*, vol. 116 (2009), pp. 585–587.

9. K. Iwata and R. Nagata, "Calculation of refractive index distribution from interferograms using the born and rytov's approximation," Jpn. J. Appl. Phys. **14**, 379–383 (1975).
10. S. Trattner, M. Feigin, H. Greenspan, and N. Sochen, "Validity criterion for the Born approximation convergence in microscopy imaging," J. Opt. Soc. Am. A **26**, 1147 (2009).
11. M. H. Jenkins and T. K. Gaylord, "Three-dimensional quantitative phase imaging via tomographic deconvolution phase microscopy," Appl. optics **54**, 9213–9227 (2015).